Journal of Materials Chemistry A

PAPER

Cite this: J. Mater. Chem. A, 2016, 4, 3872

Solvent-extraction crystal growth for highly efficient carbon-based mesoscopic perovskite solar cells free of hole conductors†

Chien-Yi Chan, Yingying Wang, Guan-Wei Wu and Eric Wei-Guang Diau*

We developed a simple drop-casting method *via* solvent extraction (SECG) to grow dense and uniform perovskite nanocrystals at room temperature for carbon-based mesoscopic solar cells free of an organic hole-transport layer. The $CH_3NH_3PbI_3$/*N*-methyl-2-pyrrolidone (NMP) precursor solution (40%) was first dripped onto a substrate with film configuration $TiO_2/Al_2O_3/C$ and infiltrated at 70 °C for 10 min. The perovskite substrate was next immersed in a bath of diethyl ether at 25 °C for 30 min. Third, the solvent-extracted substrate was stored in a dry box (humidity 50%) at 25 °C for at least 100 h to complete the crystal growth. The device performance attained a power conversion efficiency (PCE) of 12.3%, which is significantly greater than that of DMF (6.3%) and NMP (8.3%) devices using traditional thermal annealing. The SECG device displayed a superior intrinsic enduring stability: the PCE exceeded 12% for 5000 h with a maximum value of 13.3% without light-soaking at 25 °C, but the performance degraded rapidly under one-sun irradiation without encapsulation. To understand the kinetics of charge transfer and defect relaxation for the devices under investigation, we recorded transient photoluminescence decays at an excitation wavelength of 635 nm and a probe wavelength of 770 nm.

Received 29th January 2016
Accepted 5th February 2016

DOI: 10.1039/c6ta00912c

www.rsc.org/MaterialsA

Introduction

The development of all-solid-state organic–inorganic hybrid solar cells attained a new milestone when devices made of organometallic lead-halide perovskite materials exhibited superior photovoltaic performance.[1–7] Miyasaka and co-workers[8] developed the original perovskite solar cell based on a mesoporous film structure similar to a dye-sensitized solar cell. The performance of devices was advanced with various one-step[9] and two-step (sequential)[10,11] methods to control the morphology of the perovskite film, but the endurance of the device performance became a major issue for perovskite solar cells (PSCs) with organic hole-transport materials (HTMs) such as spiro-OMeTAD. To tackle this problem, the first solution was to fabricate a device with TiO_2 nanosheets without a HTM layer,[12] but the cell performance was poor. According to a one-step method, Han and co-workers in 2013[13] utilized a carbon black/graphite composite as a counter electrode to fabricate a HTM-free PSC with a three-layer film configuration TiO_2/ZrO_2/C to attain a power conversion efficiency (PCE) of 6.6%, which was significantly improved to 12.8% with the precursor solution involving an amino acid additive.[14] Intense investigations were also undertaken to fabricate carbon-based PSCs using a two-step method.[15–22] However, both methods required post-treatment for the crystal growth *via* thermal annealing (TA) at an elevated temperature (70–90 °C).

In the present work, we developed a simple method to grow uniform perovskite ($CH_3NH_3PbI_3$) nanocrystals inside mesoporous layers at room temperature using a solvent extraction approach (SECG). The concept of this method was found by Zhu and co-workers[23] to improve the morphology and crystallinity of the perovskite layer for planar heterojunction devices, similar to an idea of solvent-assisted (anti-solvent) treatment reported by Cheng, Spiccia,[24] Seok[25] and their co-workers. According to the approach of Zhu and Padture,[23] solvent–solvent extraction occurs when the perovskite substrate, prepared through one-step drop casting of a precursor solution in *N*-methyl-2-pyrrolidone (NMP), was immersed in a bath of diethyl ether (DEE) near 25 °C for ~2 min. The crystals grew when the immersed substrate was dried with blown N_2 gas near 25 °C, similarly to the gas-assisted crystallization reported by Cheng and co-workers.[26]

In our approach (Fig. 1), a perovskite solution (40% in NMP) was dripped onto the pre-heated (70 °C) mesoporous substrate containing the $TiO_2/Al_2O_3/C$ layers. After infiltration at 70 °C for 10 min, the substrate was immersed in a DEE bath at 25 °C for 30 min to complete the solvent–solvent extraction procedure. The substrate was then stored in a dry box (25 °C; humidity 50%) for several days for homogeneous crystal growth to proceed. The performance of the SECG device attained PCE

Department of Applied Chemistry and Institute of Molecular Science, National Chiao Tung University, No. 1001, Ta-Hsueh Rd., Hsinchu 30010, Taiwan. E-mail: diau@mail.nctu.edu.tw; Fax: +886-03-572-3764

† Electronic supplementary information (ESI) available. See DOI: 10.1039/c6ta00912c

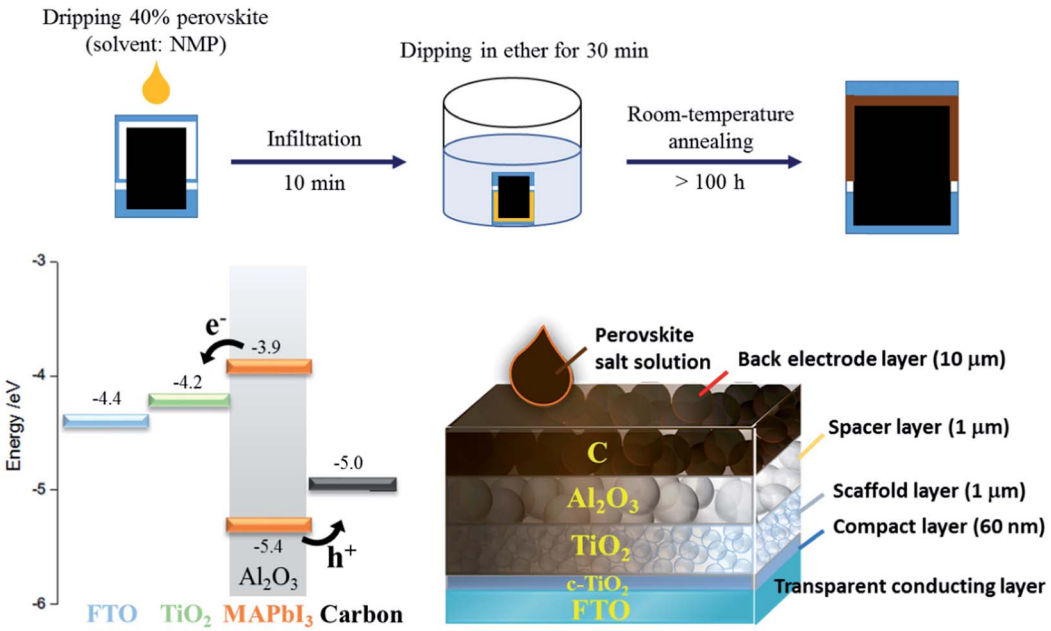

Fig. 1 Schematic illustration to fabricate a carbon-based mesoscopic perovskite ($CH_3NH_3PbI_3$) solar cell with solvent-extraction crystal growth: the corresponding device configuration and the potential levels of each component are indicated at the bottom.

12.3% after five days. In contrast, the performance of the DMF and NMP devices using a traditional one-step drop-casting method followed by TA attained PCE 6.3% and 8.3%, respectively. The maximum efficiency of the SECG device attained 13.3% during a stability test in the dark at 25 °C; the performance exceeded 12% for 5000 h. However, significant degradation of the device performance was found under strict light-soaking conditions. We demonstrate that SECG is an effective one-step approach for the fabrication of hole-conductor free carbon-based perovskite solar cells with superior device performance.

Results and discussion

Fig. 1 shows the fabrication according to the SECG method and the film configuration of the device; the corresponding potential diagram of each layer is indicated. The device was made with a thermal spray of a compact TiO_2 layer (60 nm) onto a FTO substrate, followed by screen printing of a mesoporous TiO_2 scaffold layer (~1 μm), an Al_2O_3 spacer layer (~1 μm) and a carbon electrode layer (~10 μm). To avoid current leakage *via* contact of the carbon layer with the TiO_2 layer, we used Al_2O_3 instead of ZrO_2 as the insulation layer to separate the layers between the TiO_2 scaffold and the carbon electrode. The perovskite precursor solutions were prepared in DMF (bp 153 °C) and in NMP (bp 204 °C) (concentration 40% by mass). DMF is a typical solvent to dissolve perovskite precursors (MAI and PbI_2 in molar ratio 1/1) with adequate solubility. The work of Zhu and Padture[23] inspired the selection of the NMP solvent as its high boiling point makes it suitable for solvent–solvent extraction with DEE (bp 35 °C). According to the traditional one-step drop-casting method, the precursor solutions were dripped onto the mesoporous substrate, followed by crystallization of perovskite *via* TA at 70 °C for 30 min. In contrast, instead of thermal annealing, we used a second solvent, DEE, in our SECG approach to extract the NMP solvent with the substrate immersed in the DEE bath at 25 °C for 30 min to achieve retarded crystallization, for a smooth and uniform crystal growth at room temperature for several days.

Fig. 2a and b show side-view SEM images of the DMF and NMP devices, respectively, fabricated according to one-step drop casting followed by the TA treatment; Fig. 2c and d show images of the SECG devices in the initial stage without annealing and after annealing near 25 °C for five days, respectively. The formation of perovskite crystals inside the mesoporous environment is unambiguously observed in comparison to the SEM images shown in Fig. S1, (ESI†). The perovskite infiltration in those mesoporous layers was insufficient in the DMF device, but the pore filling became significantly improved with NMP instead of DMF in the traditional one-step method. The NMP solvent with a higher boiling point assists the crystal growth *via* thermal annealing for carbon-based PSCs. Crystallization seems to occur only at the interface between the carbon and Al_2O_3 layers during the initial stage of SECG, but DEE effectively extracted the NMP solvent from the substrate in a solvent bath; the growth of perovskite nanocrystals was retarded significantly when the DEE solvent gradually evaporated from the substrate at 25 °C for a few days. The insets of Fig. 2 show the color of the perovskite substrates changing from initially pale (Fig. 2c) to black on annealing near 25 °C for five days (Fig. 2d); all unoccupied spaces in the Al_2O_3 and TiO_2 layers were firmly filled with dense perovskite crystals after this slow annealing near 25 °C.

Other than this annealing for a long period, two factors are considered here to improve the PV performance of the SECG device. First, because of the large viscosity of NMP near 25 °C,

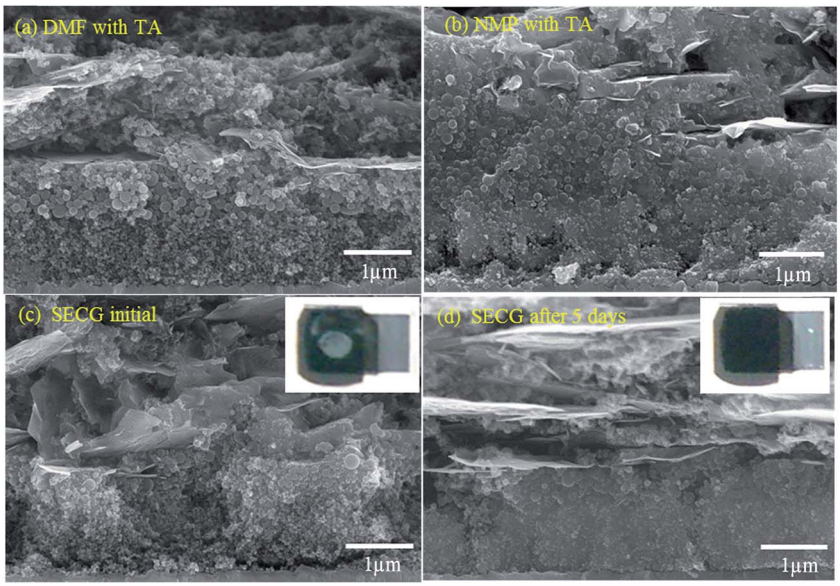

Fig. 2 Side-view SEM images showing carbon-based perovskite solar cells fabricated according to the (a) one-step thermal annealing (TA) method at 70 °C with DMF solvent, (b) one-step TA method at 70 °C with NMP solvent, (c) solvent-extraction crystal growth (SECG) before annealing near 25 °C and (d) SECG method after annealing near 25 °C for five days.

pre-heating of the substrate during the dripping and infiltration is necessary to improve the infiltration of the perovskite solution into the substrate. The effect of pre-heating from 25 to 80 °C was examined; the photovoltaic results are shown in Fig. S2 and Table S1, ESI.† The device performance increased with increasing pre-heating temperature up to 70 °C for the best performance. At 80 °C, partial crystallization might occur to prevent uniform crystal growth during the subsequent SECG procedure. Second, the amount of the precursor solution dripped onto the substrate is also an important parameter to be controlled in our SECG approach. Fig. S3, ESI,† shows three typical side-view SEM images of the devices to understand the effect of pore filling of perovskite inside those mesoporous layers. As the results in ESI Fig. S4 and Table S2† show, the optimized volume was determined to be 4 μL for a device with an active area of 0.4 cm^2, which exhibited outstanding performance with PCE 12.3% after annealing near 25 °C for five days.

Fig. 3a and b show the current–voltage characteristics and the IPCE action spectra, respectively, of the DMF, NMP and SECG devices; the corresponding PV parameters are summarized in Table 1 for comparison. The DMF device exhibited performance worse than the other two devices with the NMP solvent. The performance of the SECG device is significantly superior to that of the NMP device because the SECG approach assists the growth of dense perovskite crystals inside the mesoscopic layers, and enhances J_{SC} over the entire visible spectral region, as shown in the IPCE spectra (Fig. 3b). In Fig. 3a the reverse (solid curves) and forward (dashed curves) *J–V* scans show a slight hysteresis, which might be due to charges accumulated in the trap states of the mesoscopic interfaces. We

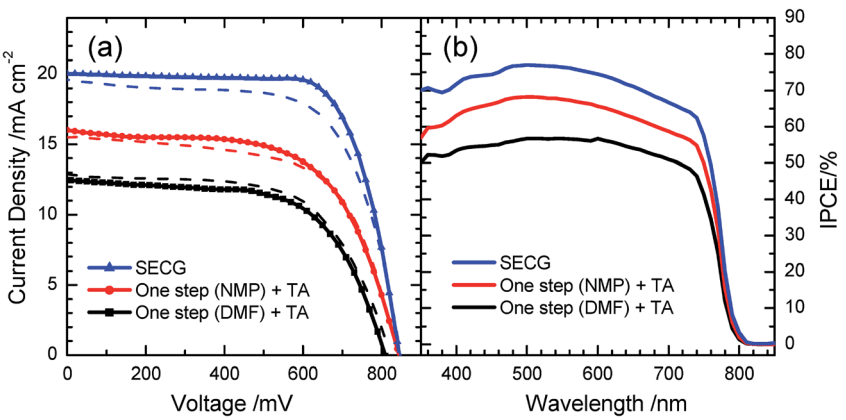

Fig. 3 Photovoltaic characteristic plots of (a) current–voltage curves (solid curves: reverse scans; dashed curves: forward scans) and (b) IPCE action spectra of carbon-based perovskite solar cells with crystals grown with solvent extraction (SECG), one-step thermal annealing (TA) method using DMF solvent and one-step TA method using NMP solvent.

Table 1 Photovoltaic parameters of carbon-based perovskite solar cells with the perovskite layer synthesized according to one-step thermal annealing (DMF), one-step thermal annealing (NMP) and solvent-extraction crystal growth (SECG), under simulated AM-1.5 G illumination (power density 100 mW cm^{-2}); active area 0.4 cm^2 covered with a metal mask 0.09 cm^2

Device	Scan direction	J_{SC}/mA cm^{-2}	V_{OC}/mV	FF	η/%
DMF	Reverse	12.54	811	0.616	6.3
	Forward	12.89	823	0.622	6.6
NMP	Reverse	13.89	825	0.725	8.3
	Forward	13.70	836	0.678	7.8
SECG	Reverse	20.04	846	0.723	12.3
	Forward	19.62	849	0.660	11.0

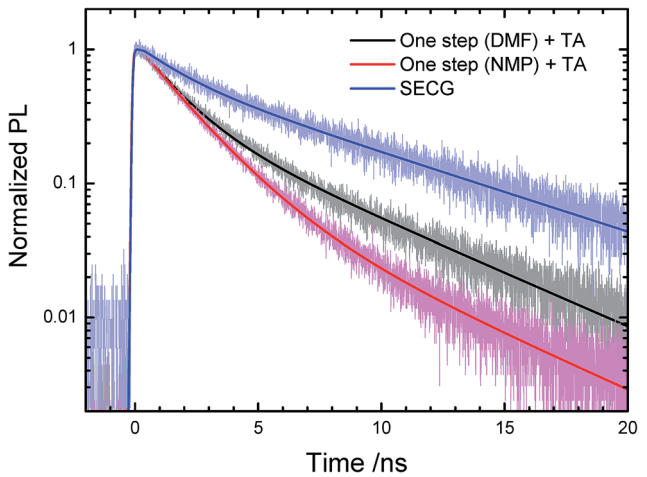

Fig. 4 Photoluminescence (PL) decays of three carbon-based perovskite solar cells showing kinetics of charge transfer and defect relaxation (excitation at 635 nm, probe at 770 nm).

Table 2 Lifetimes (relative amplitudes) of carbon-based perovskite solar cells with the perovskite layer synthesized according to one-step thermal annealing (DMF), one-step thermal annealing (NMP) and solvent-extraction crystal growth (SECG) (excitation at 635 nm, probe at 770 nm)

Device	τ_1/ns (A_1)	τ_2/ns (A_2)	τ_{PL}[a]/ns
DMF	1.50 ± 0.61 (0.39)	5.42 ± 0.13 (0.61)	3.9 ± 0.8
NMP	1.80 ± 0.03 (0.88)	5.20 ± 0.17 (0.12)	2.7 ± 0.2
SECG	1.73 ± 0.31 (0.13)	7.32 ± 0.19 (0.87)	6.6 ± 0.5

[a] The average lifetime was calculated according to a statistical definition, $\tau_{PL} = \frac{\sum A_i \tau_i^2}{\sum A_i \tau_i}$, in which τ_i are lifetimes; A_i are corresponding amplitudes of each component.

expect that dense perovskite layers in the SECG device might involve more retarded charge carriers responsible for greater hysteresis than for the other devices, explained as follows.

To understand the effect of hysteresis and the superior performance of the SECG device, we measured time-resolved photoluminescence (PL) decay with excitation at 635 nm; the PL transients were recorded at 770 nm for all the three devices. Fig. 4 shows the PL decays of the three devices. All PL transients were well fitted with a bi-exponential decay function with the corresponding lifetimes and relative amplitudes summarized in Table 2. The lifetimes of perovskite have been reported over a broad time scale depending on many factors such as excitation power,[27–29] crystallite size,[30] film configuration and morphology.[31–33] In our case, perovskite crystals of varied types were produced inside the mesoporous layers with an identical film configuration; the measured time coefficients hence reflect the nature of varied perovskite nanocrystals generated using the methods applied herein. Under the same excitation power density (0.2 μJ cm^{-2}), the non-radiative relaxation was accelerated when certain defects were involved inside the perovskite crystals, resulting in quenching of PL and decreased lifetime. For the DMF and NMP devices, the values of decay coefficients τ_1 and τ_2 are similar, but the relative amplitudes differ; for the SECG device, the second decay coefficient (τ_2 = 7.3 ns) was significantly larger than the others ($\tau_2 \sim$ 5.3 ns) and became a dominant component of the transient. As a result, the average decay coefficient of the SECG device was much larger than those of the other two devices using the traditional one-step TA method.

D'Innocenzo *et al.*[30] reported that the lifetime of perovskite depends on the size of the crystals; as small crystallites would have more surface defects than large crystallites, the lifetimes of the small crystals became smaller than those of the large crystals. In our case, perovskite crystals were produced inside the mesoporous layers containing TiO_2, Al_2O_3 and the carbon electrode. Surface defects might be involved (1) at the interfaces between the perovskite and the TiO_2/Al_2O_3/C components, and (2) in the boundaries between two perovskite grains. Because we have observed the same decay coefficient (τ_1) for all three devices, we reasonably assume that non-radiative relaxation due to charge separation occurs about ~1.5 ns and surface-defect relaxation occurs about 5–7 ns inside the carbon-based PSC. The much slower surface defect relaxation in the SECG device thus indicates that larger and denser perovskite crystals were generated with this solvent-extraction approach, consistent with the SEM images in Fig. 2. The relative amplitude of the second decay component is much greater for SECG than for other devices, indicating that the SECG approach produced large crystals with more trapped charge carriers forming excitons, which might contribute to the effect of hysteresis observed in Fig. 3a.

The concept of solvent extraction involved the use of DEE to extract NMP before crystal growth inside the mesoscopic layers. After extraction, the DEE solvent molecules were homogeneously distributed inside the mesoporous layers to attain a condition of super-saturation, similar to the case of the anti-solvent approach applied by Cheng and co-workers.[24] Zhu and co-workers[23] used the same idea of solvent extraction to immerse the perovskite/NMP substrate in DEE for only 2 min, and a uniform perovskite layer of thickness ~250 nm was produced after rapid drying with blown gaseous N_2 at room temperature. In our case, complete solvent extraction required 30 min and the formation of perovskite nanocrystals inside the

mesoporous layers was slow. This crystal-growth phenomenon can be viewed from the SEM image in Fig. 2c, for which the device performance was initially poor. As perovskite is insoluble in DEE, crystallization proceeded while the evaporation of DEE occurred slowly inside the mesoporous film.

Fig. 5 shows the photovoltaic performance of the SECG devices as a function of storage duration (time in hours) under varied experimental conditions without encapsulation. The devices were first stored in a dry box at 25 °C for the crystal growth to complete after solvent extraction. Therefore, the device performance increased substantially for the first 100 h and reached a steady level of efficiency after 120 h of storage. The long-term stability tests were then carried out for four identical SECG devices having reached the steady level of performance with a PCE in the range of 12–13% after storage for 120 h. We found that the device performance degraded quickly under one-sun irradiation at 70 °C; no appreciable efficiency can be obtained under this condition after 240 h (light soaking time 120 h). The rapid degradation of performance was also observed for the device under one-sun irradiation at 25 °C; the power conversion efficiency retained only ~1% after 480 h (light soaking time 360 h). In contrast, when the devices were stored in the dark, good performance can be retained. Under thermal stress at 70 °C without light irradiation, the efficiencies were slightly degraded but kept exceeding 10% for over 400 h. On the other hand, when the devices were stored in the dark at 25 °C, the efficiencies exceeded 12% for 5000 h with the maximum value reaching PCE 13.3%. Our stability test results thus indicate that the SECG devices without encapsulation suffered from light-soaking under one-sun irradiation. However, the SECG device exhibited a great enduring stability with high performance in the dark even under the condition of thermal stress. This result reflects the intrinsic thermal stability of carbon-based perovskite solar cells free of organic hole-transport layers, but decomposition of perovskite may occur under ambient conditions under one-sun irradiation. Further investigations are needed to improve the light-soaking stability of the SECG devices with appropriate encapsulation.

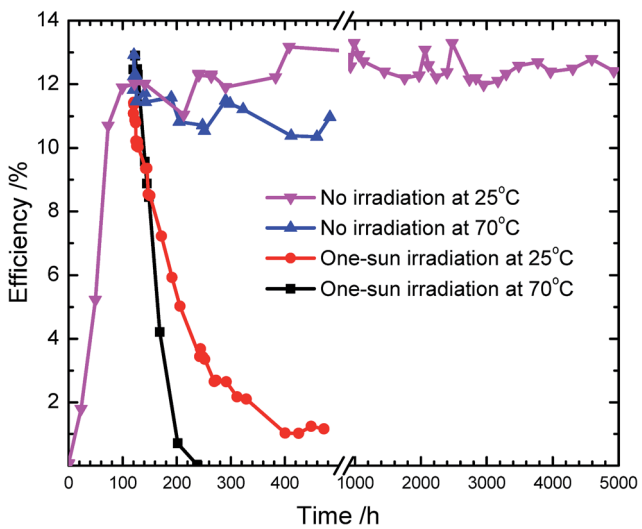

Fig. 5 Photovoltaic performance of the SECG devices as a function of time showing the enduring stabilities in the dark at 25 °C (solid inverse triangles) and 70 °C (solid triangles) as well as under one-sun irradiation at 25 °C (solid circles) and 70 °C (solid squares).

Conclusion

Perovskite solar cells (PSCs) with a mesoporous carbon layer as a p-type electrode are free of organic hole conductors and expensive rare metal layers; they are hence promising as next-generation printable photovoltaic devices. Herein we provide a simple one-step drop-casting method to fabricate highly efficient carbon-based PSCs using solvent-extraction crystal growth (SECG). Diethyl ether served as a solvent bath to extract the NMP solvent of the perovskite precursor solution to implement a homogeneous nucleation of perovskite inside the mesoporous film containing the $TiO_2/Al_2O_3/C$ layers. After solvent extraction, retarded crystallization proceeded for a few days near 25 °C to generate dense and uniform perovskite nanocrystals. The performance of the SECG device increased as the crystal grew for five days to attain a steady level with PCE 12.3%, and continued to exceed 12% for 5000 h; the maximum efficiency attained 13.3% during this stability test period under dark conditions, but the device performance degraded rapidly under one-sun irradiation. We recorded photoluminescence transients of the complete devices using the TCSPC technique, excitation at 635 nm and probe at 770 nm. Two transient components were observed with decay coefficients 1.7 and 7.3 ns, respectively. The average lifetime of the SECG device is larger than those of DMF and NMP devices fabricated according to the traditional one-step thermal annealing method, because of large and dense perovskite crystals with fewer defect states so that the SECG device showed performance better than the other two devices. Solvent extraction is a promising synthetic approach to fabricate printable mesoscopic carbon-based perovskite solar cells under ambient conditions outside a glovebox and a vacuum system with superior device performance and exceptional intrinsic enduring stability in the dark.

Experimental

Preparation of perovskite solution

Methylammonium iodide (CH_3NH_3I) was synthesized *via* the reaction of methylamine (CH_3NH_2, 21.6 mL, 40 mass% in water, Alfa Aesar) and hydriodic acid (HI, 30 mL, 57 mass% in water, with hypophosphorous acid 1.5%, Alfa Aesar) and kept stirring at 0 °C for 2 h under a N_2 atmosphere, followed by rotary evaporation to remove the solvent. The CH_3NH_3I powder was washed three times with diethyl ether (99%, anhydrous, ECHO) and dried in a vacuum oven at 50 °C overnight before use. Perovskite precursor solutions (concentration 40% by mass) were prepared in *N*-methyl-2-pyrrolidone (NMP, anhydrous, Aldrich, 1 mL) mixed with powdered CH_3NH_3I (175 mg) and PbI_2 (99%, Aldrich, 507 mg). The solution was stirred at 70 °C for 1 h before use.

Preparation of TiO_2, Al_2O_3 and carbon pastes

For octahedron-like TiO_2 nanocrystals (HD1) used for the TiO_2 layer the synthesis is reported elsewhere.[34] Both TiO_2 and Al_2O_3 pastes were prepared by mixing 15% of the TiO_2 (HD1) or the Al_2O_3 powder (Alfa Aesar) with ethyl cellulose (10%, Sigma-Aldrich) and alpha-terpineol (75%, Sigma-Aldrich). The carbon paste was prepared by mixing graphite (6 g, Homytech, Taiwan), carbon black (2.5 g, Top Nano Technology, Taiwan), Al_2O_3 (1.5 g), ethyl cellulose (10 g) and alpha-terpineol (30 g).

Preparation of electrode and devices

A dense TiO_2 compact layer was deposited on etched FTO substrates by spray pyrolysis of a titanium diisopropoxide-bis(acetylacetonate) solution (0.3 M) at 450 °C. The TiO_2, Al_2O_3 and carbon pastes as prepared were then screen-printed on the substrate layer by layer to form mesoporous films of thickness 1, 1 and 10 μm, respectively. The sintering temperatures for the TiO_2, Al_2O_3 and carbon layers were 500, 400 and 400 °C, respectively; the sintering periods were all 30 min. The perovskite precursor solution (4 μL) was dripped onto the mesoporous substrate at 70 °C and infiltrated for 10 min. The substrate was then dipped in a diethyl ether bath near 25 °C for 30 min. The film was taken from the bath and kept in a dry box (humidity 50%) for at least five days to reach the steady level of efficiency.

Characterization of film and devices

The morphology of a perovskite sample was investigated with a field-emission scanning electron microscope (FESEM, JSM-7401F, JEOL). The photovoltaic performance of the device (active area 0.4 cm^2) was measured with a solar simulator (AM 1.5 G, XES-40S1, SAN-EI). The action spectra of the incident photon to current conversion efficiency (IPCE) were recorded with a system comprising a Xe lamp (A-1010, PTi, 150 W), a monochromator (PTi, 1200 grooves mm^{-1} blazed at 500 nm) and a source meter (Keithley 2400, computer-controlled). Photoluminescence (PL) transients were recorded with a time-correlated single-photon counting (TCSPC) system (Fluotime 200, PicoQuant) with excitation at 635 nm from a picosecond pulsed-diode laser (LDH-635, PicoQuant, FWHM ~70 ps); the PL temporal profiles were collected at 770 nm.

Acknowledgements

Ministry of Science and Technology (MOST) of Taiwan supported this work with contracts NSC 102-2113-M-009-020-MY3 and NSC 103-2119-M-009-005 ET. We thank Mr. Cheng-Min Tsai for his assistance on the enduring stability test of the devices.

References

1 M. M. Lee, J. Teuscher, T. Miyasaka, T. N. Murakami and H. J. Snaith, *Science*, 2012, **338**, 643–647.
2 J. H. Rhee, C.-C. Chung and E. W.-G. Diau, *NPG Asia Mater.*, 2013, **5**, e68.
3 M. Liu, M. B. Johnston and H. J. Snaith, *Nature*, 2013, **501**, 395–398.
4 H. Zhou, Q. Chen, G. Li, S. Luo, T.-b. Song, H.-S. Duan, Z. Hong, J. You, Y. Liu and Y. Yang, *Science*, 2014, **345**, 542–546.
5 P. Gao, M. Gratzel and M. K. Nazeeruddin, *Energy Environ. Sci.*, 2014, **7**, 2448–2463.
6 W. S. Yang, J. H. Noh, N. J. Jeon, Y. C. Kim, S. Ryu, J. Seo and S. I. Seok, *Science*, 2015, **348**, 1234–1237.
7 Z. Zhou, S. Pang, Z. Liu, H. Xu and G. Cui, *J. Mater. Chem. A*, 2015, **3**, 19205–19217.
8 A. Kojima, K. Teshima, Y. Shirai and T. Miyasaka, *J. Am. Chem. Soc.*, 2009, **131**, 6050–6051.
9 H.-S. Kim, C.-R. Lee, J.-H. Im, K.-B. Lee, T. Moehl, A. Marchioro, S.-J. Moon, R. Humphry-Baker, J.-H. Yum, J. E. Moser, M. Grätzel and N.-G. Park, *Sci. Rep.*, 2012, **2**, 591.
10 J. Burschka, N. Pellet, S.-J. Moon, R. Humphry-Baker, P. Gao, M. K. Nazeeruddin and M. Gratzel, *Nature*, 2013, **499**, 316–319.
11 J.-H. Im, I.-H. Jang, N. Pellet, M. Grätzel and N.-G. Park, *Nat. Nanotechnol.*, 2014, **9**, 927–932.
12 L. Etgar, P. Gao, Z. Xue, Q. Peng, A. K. Chandiran, B. Liu, M. K. Nazeeruddin and M. Grätzel, *J. Am. Chem. Soc.*, 2012, **134**, 17396–17399.
13 Z. Ku, Y. Rong, M. Xu, T. Liu and H. Han, *Sci. Rep.*, 2013, **3**, 3132.
14 A. Mei, X. Li, L. Liu, Z. Ku, T. Liu, Y. Rong, M. Xu, M. Hu, J. Chen, Y. Yang, M. Grätzel and H. Han, *Science*, 2014, **345**, 295–298.
15 Y. Rong, Z. Ku, A. Mei, T. Liu, M. Xu, S. Ko, X. Li and H. Han, *J. Phys. Chem. Lett.*, 2014, **5**, 2160–2164.
16 M. Hu, L. Liu, A. Mei, Y. Yang, T. Liu and H. Han, *J. Mater. Chem. A*, 2014, **2**, 17115–17121.
17 L. Liu, A. Mei, T. Liu, P. Jiang, Y. Sheng, L. Zhang and H. Han, *J. Am. Chem. Soc.*, 2015, **137**, 1790–1793.
18 K. Cao, J. Cui, H. Zhang, H. Li, J. Song, Y. Shen, Y. Cheng and M. Wang, *J. Mater. Chem. A*, 2015, **3**, 9116–9122.
19 X. Xu, Z. Liu, Z. Zuo, M. Zhang, Z. Zhao, Y. Shen, H. Zhou, Q. Chen, Y. Yang and M. Wang, *Nano Lett.*, 2015, **15**, 2402–2408.
20 Z. Liu, M. Zhang, X. Xu, L. Bu, W. Zhang, W. Li, Z. Zhao, M. Wang, Y.-B. Cheng and H. He, *Dalton Trans.*, 2015, **44**, 3967–3973.
21 Y. Yang, J. Xiao, H. Wei, L. Zhu, D. Li, Y. Luo, H. Wu and Q. Meng, *RSC Adv.*, 2014, **4**, 52825–52830.
22 H. Wang, X. Hu and H. Chen, *RSC Adv.*, 2015, **5**, 30192–30196.
23 Y. Zhou, M. Yang, W. Wu, A. L. Vasiliev, K. Zhu and N. P. Padture, *J. Mater. Chem. A*, 2015, **3**, 8178–8184.
24 M. Xiao, F. Huang, W. Huang, Y. Dkhissi, Y. Zhu, J. Etheridge, A. Gray-Weale, U. Bach, Y.-B. Cheng and L. Spiccia, *Angew. Chem., Int. Ed.*, 2014, **126**, 10056–10061.
25 N. J. Jeon, J. H. Noh, Y. C. Kim, W. S. Yang, S. Ryu and S. I. Seok, *Nat. Mater.*, 2014, **13**, 897–903.
26 F. Huang, Y. Dkhissi, W. Huang, M. Xiao, I. Benesperi, S. Rubanov, Y. Zhu, X. Lin, L. Jiang, Y. Zhou, A. Gray-

Weale, J. Etheridge, C. R. McNeill, R. A. Caruso, U. Bach, L. Spiccia and Y.-B. Cheng, *Nano Energy*, 2014, **10**, 10–18.
27 G. Xing, N. Mathews, S. Sun, S. S. Lim, Y. M. Lam, M. Grätzel, S. Mhaisalkar and T. C. Sum, *Science*, 2013, **342**, 344–347.
28 S. D. Stranks, V. M. Burlakov, T. Leijtens, J. M. Ball, A. Goriely and H. J. Snaith, *Phys. Rev. Appl.*, 2014, **2**, 034007.
29 Y. Yamada, T. Nakamura, M. Endo, A. Wakamiya and Y. Kanemitsu, *J. Am. Chem. Soc.*, 2014, **136**, 11610–11613.
30 V. D'Innocenzo, A. R. Srimath Kandada, M. De Bastiani, M. Gandini and A. Petrozza, *J. Am. Chem. Soc.*, 2014, **136**, 17730–17733.
31 H.-Y. Hsu, C.-Y. Wang, A. Fathi, J.-W. Shiu, C.-C. Chung, P.-S. Shen, T.-F. Guo, P. Chen, Y.-P. Lee and E. W.-G. Diau, *Angew. Chem., Int. Ed.*, 2014, **126**, 9493–9496.
32 C. Wehrenfennig, G. E. Eperon, M. B. Johnston, H. J. Snaith and L. M. Herz, *Adv. Mater.*, 2014, **26**, 1584–1589.
33 A. Marchioro, J. Teuscher, D. Friedrich, M. Kunst, R. van de Krol, T. Moehl, M. Gratzel and J. E. Moser, *Nat. Photonics*, 2014, **8**, 250–255.
34 J.-W. Shiu, C.-M. Lan, Y.-C. Chang, H.-P. Wu, W.-K. Huang and E. W.-G. Diau, *ACS Nano*, 2012, **6**, 10862–10873.